# ON SOME ACCURATE FINITE-DIFFERENCE METHODS FOR LAMINAR FLAME CALCULATIONS

J. I. RAMOS

*Department of Mechanical Engineering, Carnegie-Mellon University, Pittsburgh, PA 15213, U.S.A.*

## SUMMARY

The ozone-decomposition flame has been studied by means of fourth- and second-order accurate schemes. The fourth-order methods include a method of lines, a time-linearization algorithm, and a majorant operator-splitting technique. The second-order schemes include two time-linearization methods which use different temporal approximations. It is shown that the fourth-order techniques yield comparable results to those obtained with very accurate finite element and adaptive grid finite-difference algorithms. The results of the second-order methods are in good agreement with second-order explicit predictor–corrector methods but predict a lower flame speed than that obtained by means of fourth-order techniques. It is also shown that the temporal approximations are not as important as the spatial approximations in flame propagation problems characterized by the presence of several small time scales.

KEY WORDS  Finite-difference  Schemes  Time-linearization  Methods  Operator-splitting Techniques  Methods of Lines  Combustion.

## INTRODUCTION

Flame propagation phenomena are characterized by the presence of very steep fronts;[1] away from the flame front, the species mass fractions and temperature profiles are almost uniform.[2] The temporal and spatial resolutions of the flame front are problems of great importance in combustion theory. In this paper we study the ozone-decomposition laminar flame. This flame has been previously studied by Bledjian,[3] Margolis,[4] Reitz[5] and Meintjes.[6] Bledjian[3] employed mass co-ordinates and reduced the set of conservation equations of species mass fractions and energy to a system of reaction–diffusion equations which were discretized in space using a second-order accurate scheme. The resulting set of ordinary differential equations was solved by means of a Runge–Kutta method and yielded a wave speed of 54·3 cm/s, although this value depended on the species used in the computation of the flame speed. Bledjian's[3] results did not exactly give a steady-state flame speed and were computed with 100 grid points.

Margolis[4] employed sixth-order B-splines, 272 collocation points, and solved the resulting set of ordinary differential equations by means of a fourth-order accurate Runge–Kutta method. His computed wave speed was 49·7 cm/s. Meintjes[6] used a second-order accurate explicit predictor–corrector method and found a flame speed of 48 cm/s. Meintjes[6] estimated that his flame speed might be in error by 2 cm/s because of the integrations required to calculate the fluid velocity. The flame speed was computed in a 121-point grid. Reitz[5] used an adaptive grid, explicit Saul'yev method and found a flame speed of 49·8 ± 0·1 cm/s when 30 grid nodes were employed in the calculations. Reitz's[5] result is in very good agreement with that obtained by Margolis.[4]

Cramarossa and Dixon–Lewis[7] have also studied the ozone-decomposition flame by means of a time-dependent numerical method.

The numerical results presented in References 1–7 as well as in this paper were calculated by employing a time-dependent approach and constant transport properties. Warnatz[8] and Heimerl and Coffee[9] have also calculated the ozone-decomposition laminar flame using transport coefficients which are a function of the temperature. Warnatz[8] employed an implicit technique while Heimerl and Coffee[9] used a relaxation method and the PDECOL package of Madsen and Sincovec.[10] This package was also employed by Margolis.[4] The results of Heimerl and Coffee[9] agreed within ± 12 per cent with those of Warnatz.[8] The differences were more remarkable in the atomic oxygen and temperature profiles and were attributed to the different input coefficients employed in the calculations.

Coffee and Heimerl[11] have also studied $H_2-O_2-N_2$ flames and performed a sensitivity analysis to determine the dependence of the laminar flame speed on the reaction pre-exponential factor, species diffusion coefficients and thermal conductivity. Coffee and Heimerl[12] also studied $H_2-O_2-N_2$ flames by means of different models for the transport properties in order to assess the effects of the diffusion coefficients and thermal conductivity on the flame speed, and concentration and temperature profiles. It was found that different transport mechanisms could yield flame speeds which could differ by about 16 per cent from each other. A model with constant transport properties was found to be in very good agreement with more sophisticated models.

Models with variable transport properties have also been employed by Tsatsaronis,[13] Smoot et al.[14], Warnatz,[15–17] Warnatz et al.[18] and Miller et al.[19] Tsatsaronis[13] employed the time-dependent method developed by Spalding et al.[20] and Stephenson and Taylor[21] to study laminar flames in $CH_4-O_2-N_2$ mixtures. Tsatsaronis[13] used a kinetic mechanism which consisted of 29 chemical reactions and found that the flame speed is very sensitive to the thermal conductivity. A variation in the transport coefficient was found to result in a 5 per cent variation in the flame speed. Smoot et al.[14] also employed the method developed by Spalding et al.[20] and used an explicit technique for the diffusion terms of the governing equations whereas a linearized implicit method was employed for the kinetic terms. Smoot et al.[14] studied the effects of the pressure, initial methane concentration and temperature, reaction rate constants and transport coefficients on a kinetic mechanism which consisted of 28 reactions and reported good comparisons with the available experimental data.

Warnatz[15] has studied flames in $H_2-O_2-N_2$ mixtures by means of 18 chemical reactions using variable transport properties and an implicit method which yields a tridiagonal system of linear equations. The same numerical method was employed to study the structure of hydrocarbon-air,[16] and alkene and acetylene flames.[17,18] The numerical studies of Coffee and Heimerl[9,11,12] and Warnatz[8,15–18] can yield very important information concerning the effects of the transport properties, kinetics, and initial temperature, pressure and concentration on the propagation of laminar flames, their structure and speed. They can also provide information about the importance of certain chemical reactions in flame propagation problems under different conditions. A sophisticated steady-state model has been developed by Miller et al.[19] to explain a wide variety of experimental results. The model is based on the steady-state conservation equations of mass and energy and employs a damped Newton method and/or a modified Newton method. The calculations are started in a coarse grid which is determined from experimental results and refined in steep regions until a specified convergence criterion is achieved.

In this paper the ozone-decomposition laminar flame is studied by means of fourth- and second-order accurate finite-difference schemes. The fourth-order schemes include a time-linearization algorithm, a method of lines and a majorant operator-splitting technique. The second-order

methods are based on time-linearization but employ first- and second-order temporal approximations. All of these finite-difference methods use fixed grids, are aimed at assessing the influence of different spatial and temporal approximations on the computed flame speeds, and their results are compared with those obtained by using finite element, adaptive grid finite-difference, and fixed-node finite-difference algorithms. The calculations have been performed with constant properties and are compared with those reported in References 1–7.

## PROBLEM FORMULATION

Consider the propagation of a laminar flame through an unconfined mixture in one-dimensional space, $-\infty < x < \infty$, where the upstream and downstream locations correspond to unburned and burned gases, respectively. Assuming that the laminar flame speed is small compared with the velocity of sound in the unburned gases, the pressure can be assumed uniform and constant. Assuming also that the specific heats at constant pressure of the different species are equal and constant, neglecting the viscous dissipation terms, and assuming that the species diffusion coefficients are equal, the equations governing the conservation of mass, momentum, energy and species mass fractions can be written as[22]

$$\frac{\partial \rho}{\partial t} + \frac{\partial(\rho u)}{\partial x} = 0 \tag{1}$$

$$p = \text{constant} = p_0 \tag{2}$$

$$\rho C_p \left[ \frac{\partial T}{\partial t} + u \frac{\partial T}{\partial x} \right] = \frac{\partial}{\partial x} \left( \lambda \frac{\partial T}{\partial x} \right) - \sum_{i=1}^{N} \omega_i h_i^0 \tag{3}$$

$$\rho \left[ \frac{\partial Y_j}{\partial t} + u \frac{\partial Y_j}{\partial x} \right] = \frac{\partial}{\partial x} \left( \rho D \frac{\partial Y_j}{\partial x} \right) + \omega_j, \quad j = 1, \ldots, N-1 \tag{4}$$

$$Y_N = 1 - \sum_{i=1}^{N-1} Y_i \tag{5}$$

$$p = \rho \tilde{R} T \sum_{i=1}^{N} \frac{Y_i}{W_i} \tag{6}$$

where $\rho$ is the density; $u$, the velocity; $p$, the pressure; $t$, the time; $x$, the axial co-ordinate; $p_0$, the upstream pressure; $C_p$, the specific heat at constant pressure; $T$, the temperature; $\lambda$, the thermal conductivity; $N$, the number of species; $\omega_i$, the reaction rate of species $i$; $h_i^0$, the enthalpy of formation of species $i$; $Y_j$, the mass fraction of species $j$; $D$ is the species diffusion coefficient; $W_i$, the molecular weight of species $i$; $\tilde{R}$, the universal gas constant.

Equations (1)–(4) can be simplified by introducing mass (or Lagrangian) co-ordinates[1–4] by means of the mapping $(t, x) \rightarrow (t^*, \Psi)$ defined by

$$t^* = t \tag{7}$$

$$\frac{\partial \Psi}{\partial x} = \rho \tag{8}$$

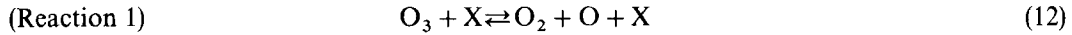$$\frac{\partial \Psi}{\partial t} = -\rho u \tag{9}$$

Making the above transformation of co-ordinates we obtain

$$\frac{\partial T}{\partial t^*} = \frac{\rho^2 D}{Le} \frac{\partial^2 T}{\partial \Psi^2} - \sum_{i=1}^{N} \frac{\omega_i}{\rho C_p} h_i^0 \tag{10}$$

$$\frac{\partial Y_j}{\partial t^*} = \rho^2 D \frac{\partial^2 Y_j}{\partial \Psi^2} + \frac{\omega_j}{\rho}, \quad j = 1, \ldots, N-1 \tag{11}$$

where $\rho^2 D$ has been assumed constant and where $Le$ is the Lewis number. In our calculations $p_0 = 0.821$ atm, $Le = 1$, $C_p = 0.2524$ cal/gr/°K, and $\rho^2 D = 4.3358 \times 10^{-7}$ gr²/cm⁴/s.

In order to fully specify the problem formulation we need to define the reaction rate terms $\omega_i$ and the enthalpies of formation $h_i^0$. We thus consider the following chemical reaction mechanism[4]

(Reaction 1)                    $O_3 + X \rightleftarrows O_2 + O + X$                    (12)

(Reaction 2)                    $O + O_3 \rightleftarrows 2O_2$                    (13)

(Reaction 3)                    $O_2 + X \rightleftarrows 2O + X$                    (14)

such that the rate of production $\omega_i$ of species $i$ is given by the law of mass action as

$$\omega_i = W_i \sum_{r=1}^{3} (v_{i,r}'' - v_{i,r}') \left[ K_{fr} \prod_{m=1}^{M} c_m^{v_{i,r}'} - K_{br} \prod_{m=1}^{M} c_m^{v_{i,r}''} \right] \tag{15}$$

where $v_{i,r}$ is the stoichiometric coefficient of species $i$ in reaction $r$; $K_{fr}$ and $K_{br}$ are the specific rate constants for the forward and backward modes of reaction $r$; ' and " denote reactants and products; and $c$ are the concentrations which are related to the mass fractions by

$$c_i = \rho Y_i / W_i \tag{16}$$

The general form of the specific rate constants is

$$K_r = A_r T^\beta \exp(-E_r / \tilde{R} T) \tag{17}$$

where $A_r$, $\beta$ and $E_r$ are the pre-exponential factor, the temperature exponent and the activation energy, respectively. The values of these parameters can be found in Reference 4 and are not repeated here. It should be pointed out that in equations (12) and (14) X stands for any of the three species, i.e. $O$, $O_2$ or $O_3$, so that equations (12)–(14) represent a system of seven reversible chemical reactions with three species.

Equations (10) and (11) can be written in vector form as

$$\frac{\partial A}{\partial t} = a \frac{\partial^2 A}{\partial \Psi^2} + S \tag{18}$$

where

$$a = \rho^2 D, A = (T, Y_1, Y_2)^T, S = \left( -\sum_{i=1}^{N} \frac{\omega_i h_i^0}{\rho C_p}, \frac{\omega_1}{\rho}, \frac{\omega_2}{\rho} \right)^T$$

and the superscript T denotes transpose.

## THE FINITE-DIFFERENCE SCHEMES

Several finite-difference schemes have been employed to solve equation (18). The methods include a fourth-order accurate method of lines, a fourth-order accurate majorant operator-splitting technique and three time-linearization schemes. These include first- and second-order accurate time approximations, and second- and fourth-order accurate spatial discretizations. The

aforementioned schemes use different spatial and temporal approximations and are employed here to assess the influence of different truncation errors and numerical schemes on the numerical calculations. A brief description of the finite-difference methods follows.

## A fourth-order accurate method of lines

In this technique equation (18) is discretized as

$$\frac{\mathrm{d}A_i}{\mathrm{d}t^*} = \frac{a}{12\Delta\Psi^2}[-A_{i-2} + 16A_{i-1} - 30A_i + 16A_{i+1} - A_{i+2}] + S_i \tag{19}$$

where the second-order spatial derivative has been discretized, but the time derivative has been kept continuous. This yields a system of coupled non-linear ordinary differential equations which have been solved by means of a fourth-order accurate Runge–Kutta method. The spatial derivative discretization has an associated truncation error equal to $O(\Delta\Psi^4)$, where $O(\Delta\Psi^4)$ denotes terms of the order of $\Delta\Psi^4$. Thus the total truncation error of this scheme is $O(\Delta t^{*4}, \Delta\Psi^4)$.

## A fourth-order accurate majorant operator-splitting method

In equation (18) two time scales are present: the characteristic diffusion and reaction times. The non-linear reaction terms, $S_i$ can be treated separately from the diffusion terms as long as they remain coupled. This allows us to split the reaction–diffusion operator of equation (18) into two operators: a diffusion operator and a reaction operator. This procedure is generally known as the method of fractional steps and is due to Yannenko.[23] In each fractional step one term of equation (18) is considered alone, while the remaining terms are ignored. Equation (18) is thus split into a reaction and a diffusion operator as follows:

$L_R$ (reaction operator): $\qquad L_R(A_i) = \dfrac{\mathrm{d}A_i}{\mathrm{d}t^*} - S_i = 0 \tag{20}$

$L_D$ (diffusion operator): $\qquad L_D(A_i) = \dfrac{\partial A_i}{\partial t^*} - a\dfrac{\partial^2 A_i}{\partial\Psi^2} = 0 \tag{21}$

The solution is then advanced from time $(t^*)^n$ to $(t^*)^{n+1}$ by the sequence

$$A_i^{n+1} = L_D[L_R(A_i^n)] \tag{22}$$

In our calculations equation (20) was first integrated using a fourth-order accurate Runge–Kutta method since it represents a system of coupled non-linear ordinary differential equations. The solution of equation (20) was denoted by $\bar{A}_i$; this value was then used to solve equation (21) which was discretized by means of a compact three-point scheme[24] for the diffusion terms. The discretization of the diffusion terms is given by

$$\frac{\partial^2 A_i}{\partial\Psi^2} = \frac{1}{\Delta\Psi^2}\frac{\delta^2}{1 + \delta^2/12}A_i + O(\Delta\Psi^4) \tag{23}$$

where $\delta^2$ is the second-order accurate finite-difference operator defined by

$$\delta^2 A_i = A_{i+1} - 2A_i + A_{i-1} \tag{24}$$

Equation (21) is then discretized as

$$\frac{A_i^{n+1} - \bar{A}_i}{\Delta t^*} = \frac{a}{\Delta\Psi^2}\frac{\delta^2}{1 + \delta^2/12}\left[\frac{A_i^{n+1} + \bar{A}_i}{2}\right] \tag{25}$$

which can be written as

$$\left(1 + \frac{\delta^2}{12}\right)(A_i^{n+1} - \bar{A}_i) = \gamma\delta^2[A_i^{n+1} + \bar{A}_i]$$  (26)

where $\gamma = a\Delta t^*/2\Delta\Psi^2$.

Equation (26) represents a system of linear finite-difference equations which can be written as a tridiagonal matrix. This matrix was solved by means of the standard tridiagonal matrix algorithm.

It should be pointed out that during the integration of the reaction operator (20) the time step was varied as necessary to maintain a specified accuracy and was, in general smaller (by about a factor of 3) than the time step $\Delta t^* = (t^*)^{n+1} - (t^*)^n$. Larger time steps were also used when solving the reaction operator equation but resulted in uncoupling between the reaction and diffusion processes and yielded, after some time, complete instability. It was found that in order to maintain a prescribed accuracy the time step used in the solution of the reaction operator should be smaller than one third of $\Delta t^*$.

### Time-linearization schemes

Equation (18) represents a system of coupled non-linear partial differential equations whose solution may be accelerated by means of linearization schemes. In this section we describe some time-linearization methods which have been employed to solve equation (18). These methods use different spatial and temporal approximations and are aimed at assessing the influence of several truncation errors on the ozone-decomposition laminar flame speed. We use time-linearization as opposed to iteration-linearization schemes in which the non-linear terms (in our case, the reaction terms, $S_i$) are linearized with respect to the previous iteration. This linearization in iteration space results in a system of linear, coupled finite-difference equations which may be solved by means of iterative or block methods. In time-linearization methods, however, the non-linear terms are linearized with respect to the previous time values. This results in a system of linear finite-difference equations. Iteration-linearization methods yield equations which have to be iterated to obtain the solution. Time-linearization schemes do not require iterations to converge within the time step. Iteration-linearization schemes are generally associated with the work of Bellman and Kalaba;[25] time-linearization methods are normally associated with the works of Briley and McDonald[26] and Beam and Warming.[27]

In what follows we introduce several time-linearization schemes that yield systems of tridiagonal matrices whereas the Briley and McDonald[26] method yields a block tridiagonal matrix.

Equation (18) was discretized using a first-order accurate method as

$$A_i^{n+1} - A_i^n = 2\gamma\delta^2 A_i^{n+1} + \Delta t^* S_i^{n+1}$$  (27)

The reaction term was linearized as

$$S_i^{n+1} = S_i^n + \text{diag}\left(\frac{\partial S}{\partial A}\right)_i^n (A_i^{n+1} - A_i^n)$$  (28)

which, when substituted into equation (27), yields a tridiagonal matrix for the unknowns $A_i$. The matrix diag $(\partial S/\partial A)$ is diagonal and signifies that the linearization of the source term $S_i$ is only performed with respect to that variable whose equation is being solved. That means that when equation (28) is substituted into equation (27) there results a system of linear uncoupled equations for the temperature, ozone mass fraction and oxygen mass fraction. This system was written as a tridiagonal matrix and solved by means of the standard tridiagonal matrix algorithm. Equations (27) and (28) define our first time-linearization algorithm whose truncation error is $O(\Delta t^*, \Delta\Psi^2)$.

Equation (18) can be discretized by using a Crank–Nicolson scheme as

$$A_i^{n+1} - A_i^n = \gamma\delta^2(A_i^{n+1} + A_i^n) + \frac{\Delta t^*}{2}(S_i^{n+1} + S_i^n) \tag{29}$$

Introducing equation (28) into equation (29), a system of linear, uncoupled finite-difference equations is obtained. This system can be solved by means of the standard tridiagonal matrix algorithm. Equations (28) and (29) represent our second time-linearization scheme whose truncation error is $O(\Delta t^{*2}, \Delta\Psi^2)$.

If instead of substituting equation (28) into equation (29) we substitute

$$S_i^{n+1} = S_i^n + \left(\frac{\partial S}{\partial A}\right)_i^n (A_i^{n+1} - A_i^n) \tag{30}$$

we obtain a system of linear, coupled equations for the temperature and mass fractions of oxygen and ozone. This system can be written as a block tridiagonal matrix which can be solved directly by using $LU$ decomposition. Introducing equation (30) into equation (29) results in a time-linearization algorithm which is associated with Briley and McDonald.[26] It should be pointed out that in equation (30) the linearization of the non-linear terms is performed with respect to all the independent variables, whereas that of equation (28) is only performed with respect to one variable. These two linearization methods yield systems of coupled and uncoupled linear algebraic equations, respectively. Thus, although in time-linearization schemes the finite-difference equations are linear, one has the option to eliminate their coupling by considering only the diagonal elements of the Jacobian matrix $(\partial S/\partial A)$ as indicated in equation (28).

Our third time-linearization method employs the compact three-point approximation given by equation (23) for the diffusion terms. This results in the following system of finite-difference equations

$$A_i^{n+1} - A_i^n = \gamma\frac{\delta^2}{1 + \delta^2/12}[A_i^n + A_i^{n+1}] + \frac{\Delta t^*}{2}[S_i^n + S_i^{n+1}] \tag{31}$$

which can be arranged as

$$\left(1 + \frac{\delta^2}{12}\right)(A_i^{n+1} - A_i^n) = \gamma\delta^2(A_i^n + A_i^{n+1}) + \frac{\Delta t^*}{2}\left(1 + \frac{\delta^2}{12}\right)[S_i^n + S_i^{n+1}] \tag{32}$$

Substituting equation (28) into equation (32) results in a system of non-linear, uncoupled finite-difference equations whose truncation error is $O(\Delta t^{*2}, \Delta\Psi^4)$. It should be pointed out that equation (31) corresponds to a Crank–Nicolson discretization algorithm where the second-order spatial derivative has been replaced by a three-point compact, fourth-order accurate approximation. Equations (28) and (32) define our third time-linearization algorithm.

## PRESENTATION AND DISCUSSION OF RESULTS

The aforementioned finite-difference schemes were employed to compute the ozone-decomposition laminar flame speed. An initial flame front was assumed to propagate into an unburned mixture composed of 25 per cent (by volume) of $O_3$ and 75 per cent of $O_2$. The temperature and pressure of the unburned mixture are $T_0 = 300\,K$ and $p_0 = 0{\cdot}821$ atm, respectively. The finite-difference calculations were performed with 121 grid points and up to the same time, i.e. $t = 2057\,\mu s$, in all the methods employed. The infinite domain $-\infty < \Psi < \infty$ was truncated in such a way that the locations of the upstream and downstream boundaries did not affect the computed

results. The truncated domain corresponds to $0 \leq \Psi \leq \Psi_T = 2.5239 \times 10^{-4}\,g/cm^2$; the downstream location of the truncated domain corresponds to that of Margolis.[4] Initially the following profiles were assumed:

$$Y_1 = \begin{cases} 1/3 & 0 \leq \Psi/\Psi_0 \leq 8.8 \\ \dfrac{1}{3} - \dfrac{1}{3}\cos^5\left[\dfrac{\pi}{2}\dfrac{\Psi_T - \Psi}{1.2\Psi_0}\right], & 8.8 \leq \Psi/\Psi_0 \leq 10 \end{cases} \tag{33}$$

$$Y_2 = \begin{cases} 2/3 & 0 \leq \Psi/\Psi_0 \leq 8.8 \\ \dfrac{2}{3} + \left(\dfrac{1}{3} - 0.0005\right)\cos^5\left[\dfrac{\pi}{2}\dfrac{\Psi_T - \Psi}{1.2\Psi_0}\right], & 8.8 \leq \Psi/\Psi_0 \leq 10 \end{cases} \tag{34}$$

$$T/T_0 = \begin{cases} 1.0 & 0 \leq \Psi/\Psi_0 \leq 8.8 \\ 1.0 + 3.166667\cos^5\left[\dfrac{\pi}{2}\dfrac{\Psi_T - \Psi}{1.2\Psi_0}\right], & 8.8 \leq \Psi/\Psi_0 \leq 10 \end{cases} \tag{35}$$

where $\Psi_0 = \Psi_T/50$ and $Y_1$ and $Y_2$ are the mass fractions of ozone ($O_3$) and oxygen ($O_2$). The mass fraction of atomic oxygen can be calculated from equation (5).

Equation (18) was solved for the $O_3$, $O_2$ and temperature since the atomic oxygen mass fraction is very small. The calculations were performed in non-dimensional co-ordinates similar to those of Margolis.[4]

Some sample results computed with the fourth-order accurate majorant operator-splitting method are shown in Figures 1–8. These Figures show the mass fraction and temperature profiles as a function of $\Psi/\Psi_0$. The $x$ co-ordinate was calculated from equation (8) as

$$x = \int_{-\infty}^{\Psi} \frac{d\Psi}{\rho} \tag{36}$$

As mentioned before the computational domain $-\infty \leq \Psi \leq \infty$ was truncated to $0 \leq \Psi \leq \Psi_T$ so that the lower limit of integration in equation (36) corresponds to 0. Equation (36) can also be written as

$$X = x\frac{\rho_0}{\Psi_0} = \int_0^{\Psi} \frac{d(\Psi/\Psi_0)}{\rho/\rho_0} \tag{37}$$

which is the non-dimensional co-ordinate used in Figures 9–16. In the above expressions the subscript stands for conditions upstream of the flame front, i.e. for conditions at $\Psi = -\infty$.

Figures 1–8 show the species mass fraction and temperature profiles at different times as a function of the mass co-ordinate $\Psi$ which has been normalized by $\Psi_0$. These Figures illustrate the early flame development, the diffusion of heat and the approach to the final steady-state profiles. Similar trends are observed in Figures 9–16 which show the species mass fraction and temperature profiles as a function of $X$ (equation (37)). The results shown in Figures 1–16 were computed with the fourth-order accurate majorant operator-splitting method. Calculations were also performed with the fourth-order accurate method of lines, and the three time-linearization schemes (the time-linearization method of Briley and McDonald[26] was not used in the present calculations) but could not be distinguished from those shown in Figures 1–16. There are, however, some differences in the computed flame speeds as will be shown later. Figures 1–16 were compared with those of Bledjian,[3] Margolis,[4] Reitz[5] and Meintjes.[6] A comparison of our results with those of Margolis,[4] who studied a premixed laminar flat flame by means of a finite-element method and employed 270 breakpoints, shows very few differences except for those in the atomic oxygen. Margolis's[4] atomic
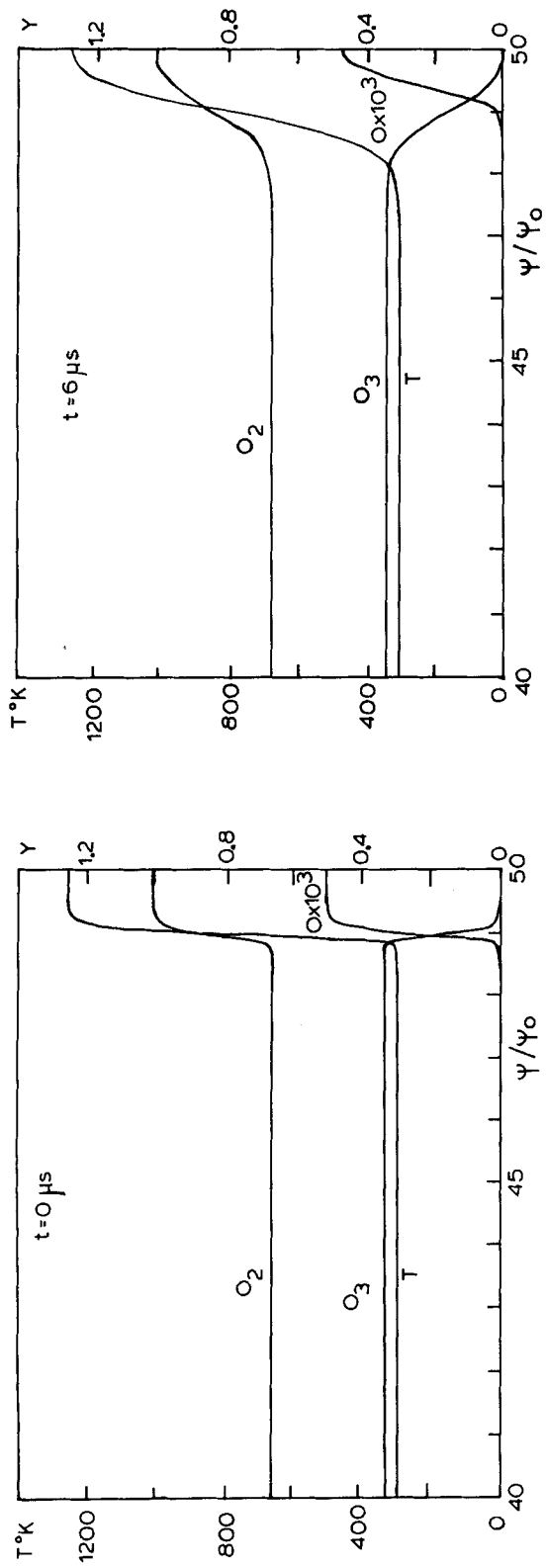
**Figure 1** (t = 0 μs): axes T°K (1200, 800, 400, 0), $\Psi/\Psi_o$ (40, 45, 50), Y (1.2, 0.8, 0.4, 0); curves $O_2$, $O_3$, $T$, $O\times10^3$

**Figure 2** (t = 6 μs): axes T°K (1200, 800, 400, 0), $\Psi/\Psi_o$ (40, 45, 50), Y (1.2, 0.8, 0.4, 0); curves $O_2$, $O_3$, $T$, $O\times10^3$

**Figure 3** (t = 29 μs): axes T°K (1200, 800, 400, 0), $\Psi/\Psi_o$ (40, 45, 50), Y (1.2, 0.8, 0.4, 0); curves $O_2$, $O_3$, $T$, $O\times10^3$

**Figure 4** (t = 59 μs): axes T°K (1200, 800, 400, 0), $\Psi/\Psi_o$ (40, 45, 50), Y (1.2, 0.8, 0.4, 0); curves $O_2$, $O_3$, $T$, $O\times10^3$

Figure 1. Species mass fraction and temperature profiles as a function of $\Psi/\Psi_o(t=0\,s)$
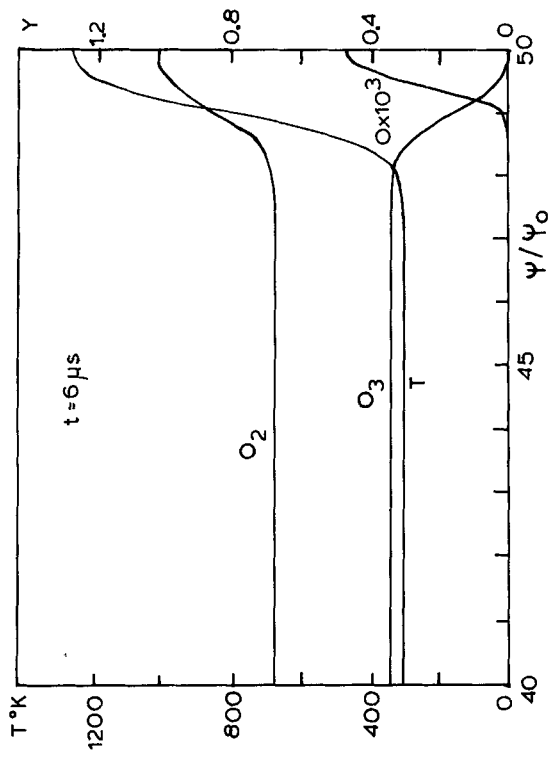
Figure 2. Species mass fraction and temperature profiles as a function of $\Psi/\Psi_0(t=6\,\mu s)$
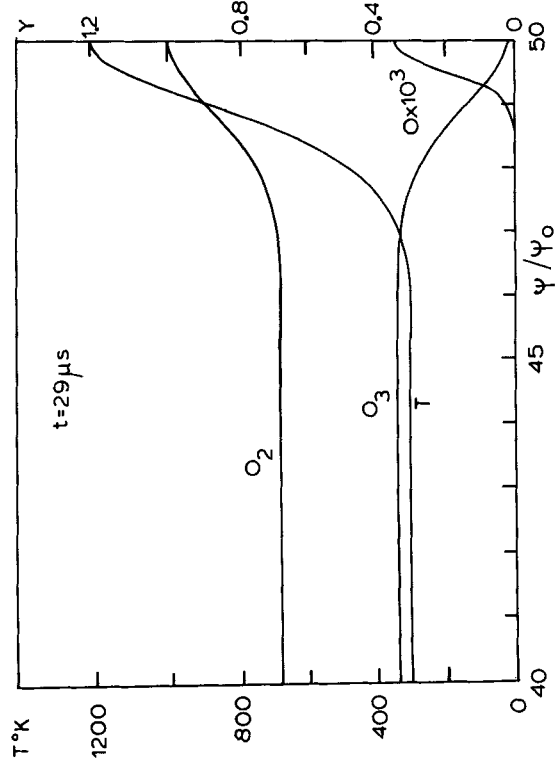
Figure 3. Species mass fraction and temperature profiles as a function of $\Psi/\Psi_0(t=29\,\mu s)$.
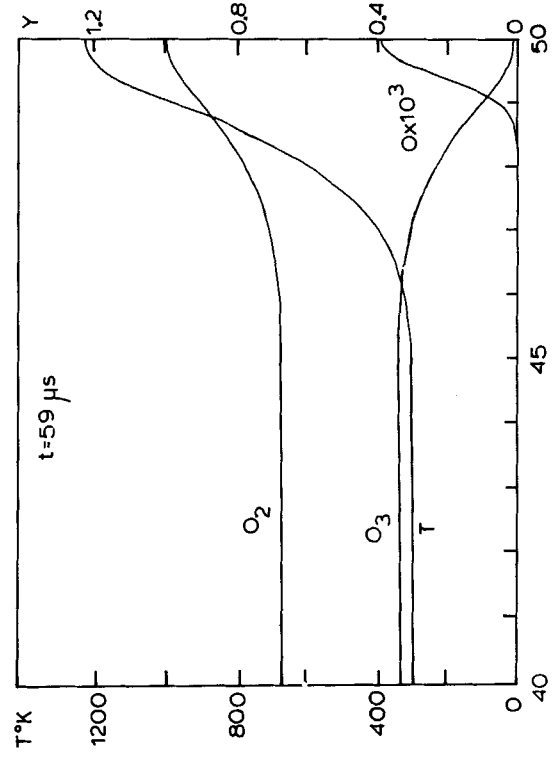
Figure 4. Species mass fraction and temperature profiles as a function of $\Psi/\Psi_0(t=59\,\mu s)$
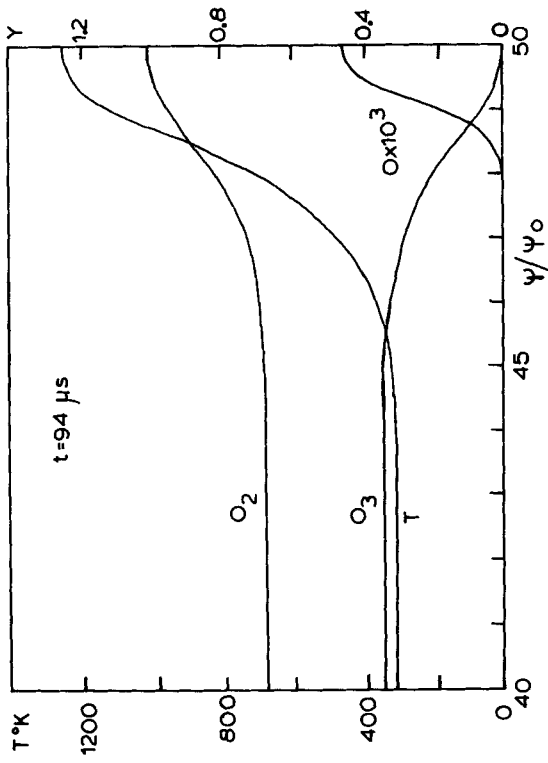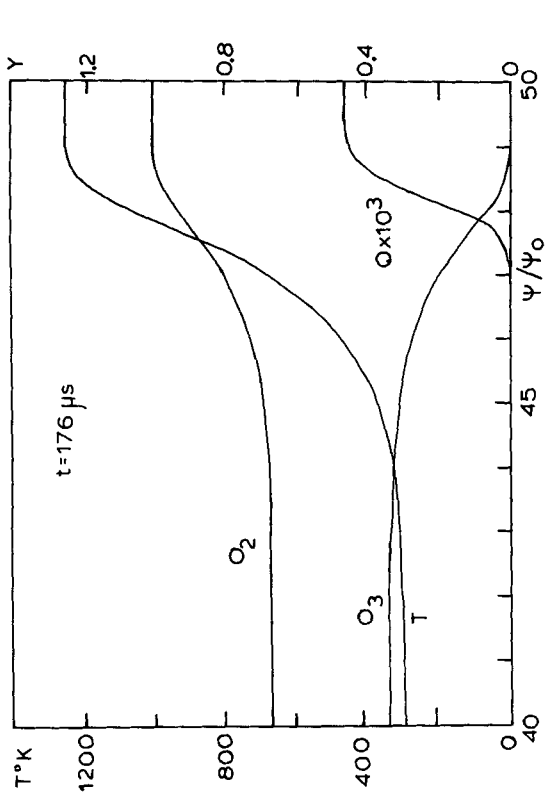
Figure 5. Species mass fraction and temperature profiles as a function of $\Psi/\Psi_0(t = 94\ \mu s)$    Figure 6. Species mass fraction and temperature profiles as a function of $\Psi/\Psi_0(t = 176\ \mu s)$
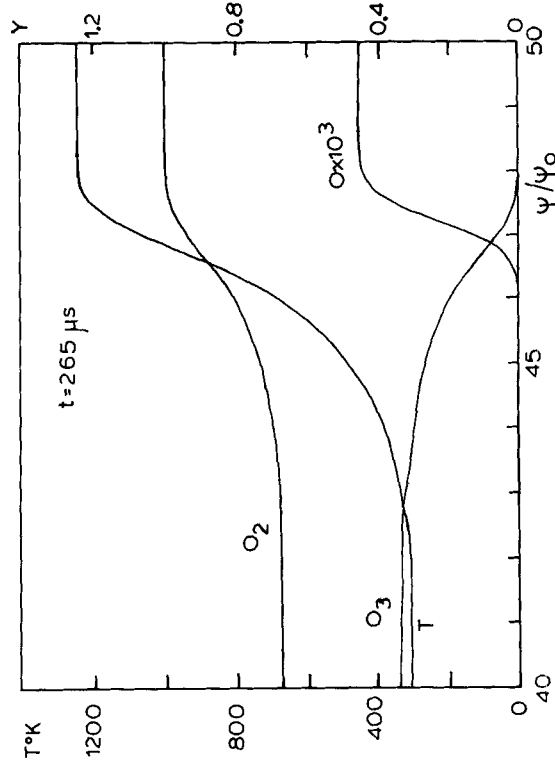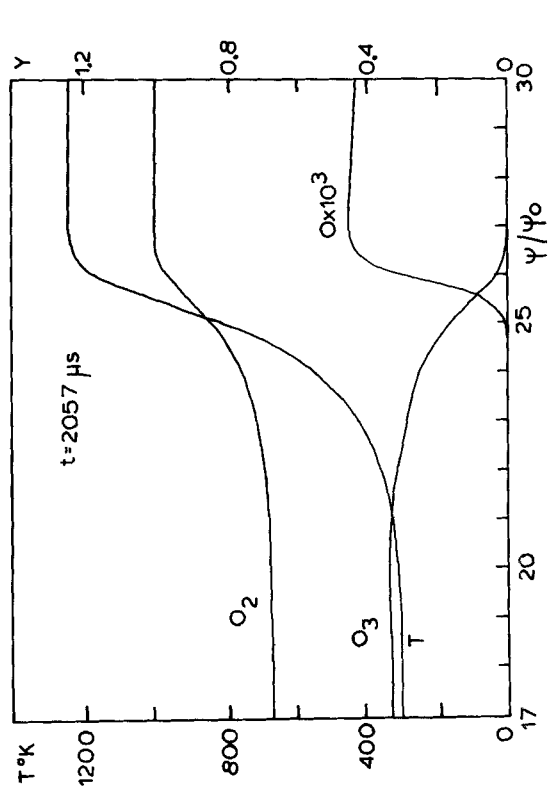
Figure 7. Species mass fraction and temperature profiles as a function of $\Psi/\Psi_0(t = 265\ \mu s)$    Figure 8. Species mass fraction and temperature profiles as a function of $\Psi/\Psi_0(t = 2057\ \mu s)$
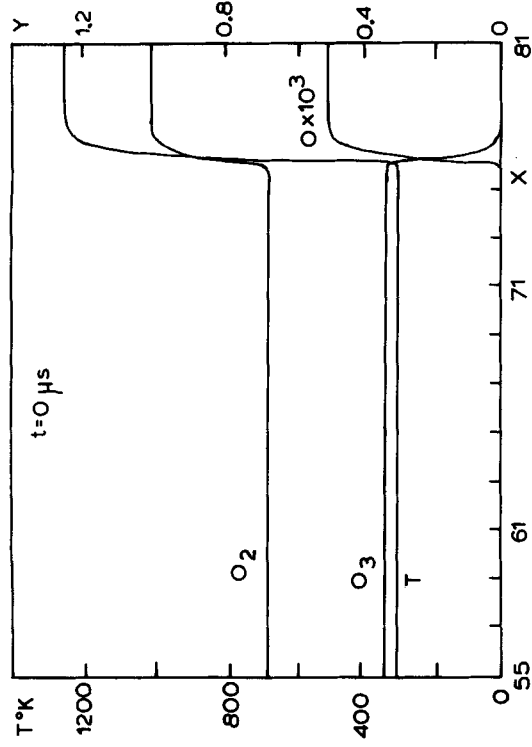
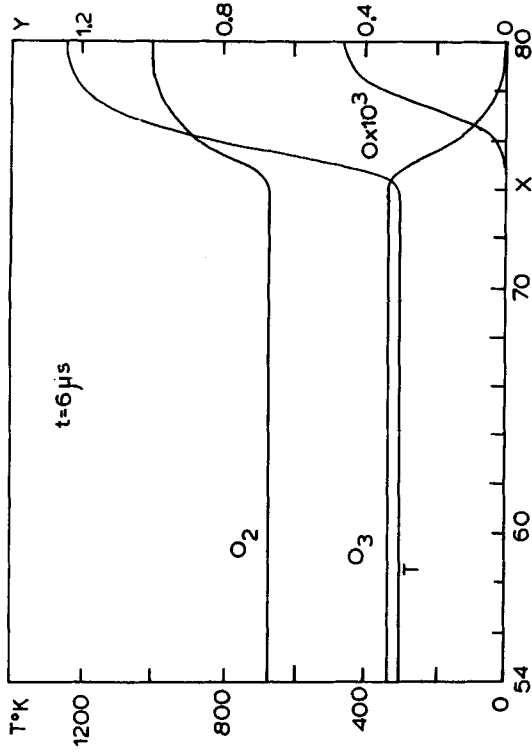Figure 9. Species mass fraction and temperature profiles as a function of $X(t = 0\,s)$    Figure 10. Species mass fraction and temperature profiles as a function of $X(t = 6\,\mu s)$
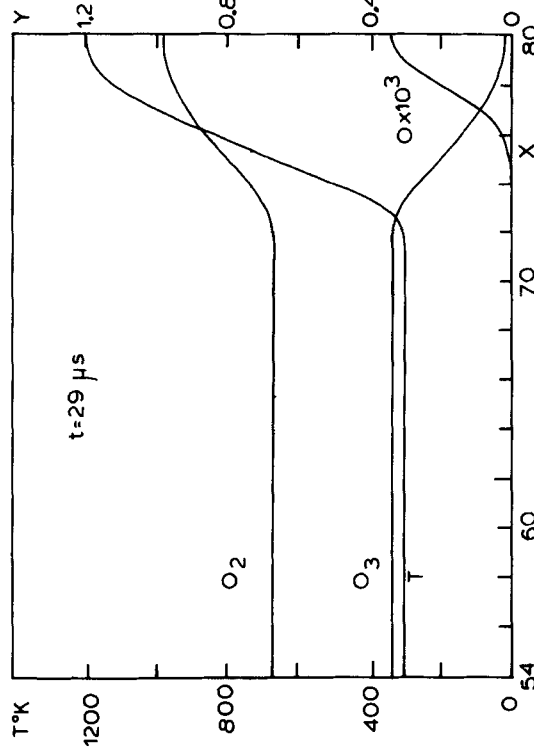
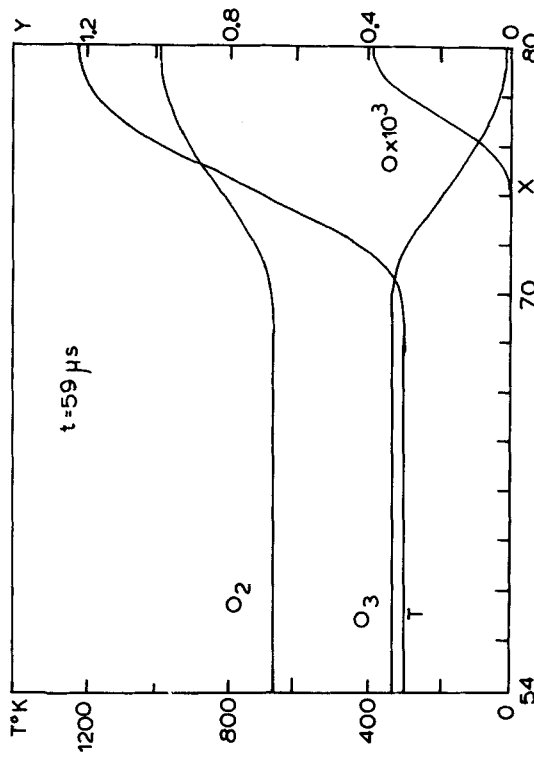Figure 11. Species mass fraction and temperature profiles as a function of $X(t = 29\,\mu s)$    Figure 12. Species mass fraction and temperature profiles as a function of $X(t = 59\,\mu s)$

Figure 13. Species mass fraction and temperature profiles as a function of $X(t = 94\,\mu s)$

Figure 14. Species mass fraction and temperature profiles as a function of $X(t = 176\,\mu s)$
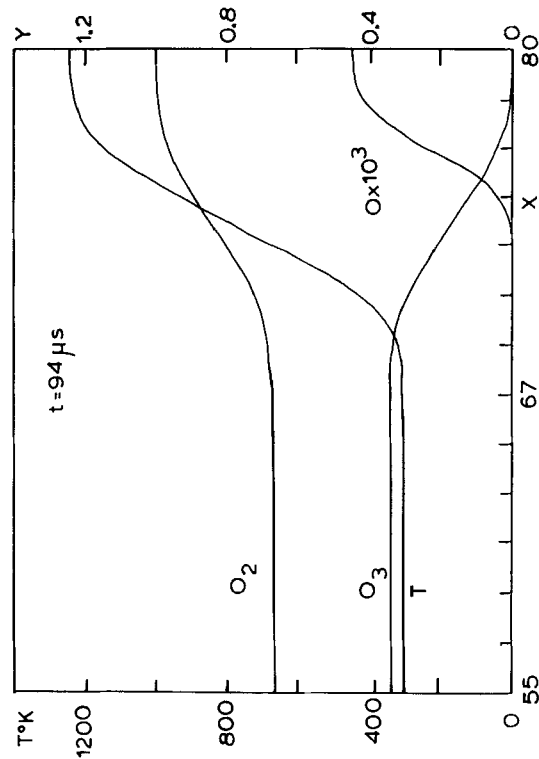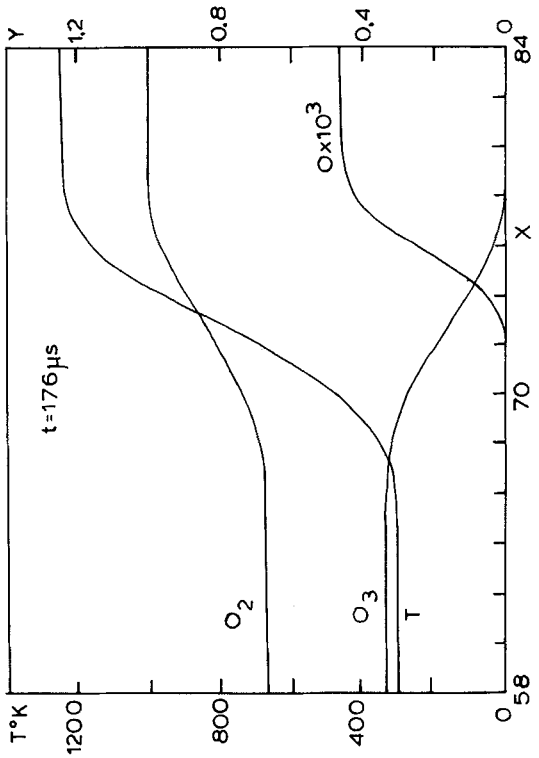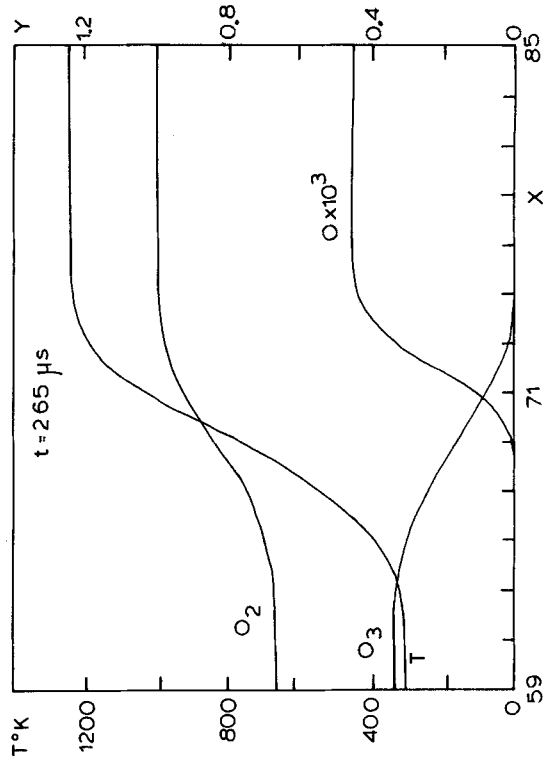
Figure 15. Species mass fraction and temperature profiles as a function of $X(t = 265\,\mu s)$
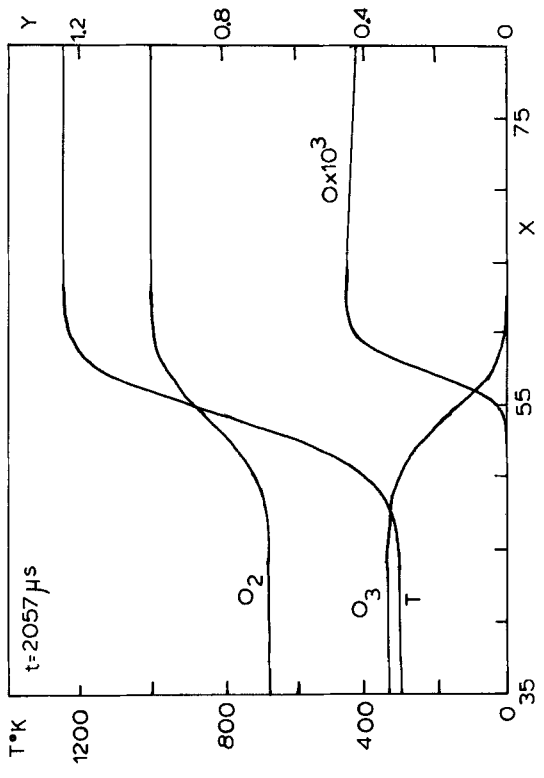
Figure 16. Species mass fraction and temperature profiles as a function of $X(t = 2057\,\mu s)$

oxygen profile in the burned gas region decreases slightly faster than the one computed here. This can easily be appreciated by comparing our Figures 8 and 16 with his Figures 1 and 2.

A comparison of our results with those of Bledjian,[3] who used a second-order accurate method of lines, shows a significant difference in the profile of atomic oxygen. Margolis[4] claimed that the difference between his results and those of Bledjian[3] could be explained in view of the multiple time scales involved in the problem, for a consideration of the rates at which each of the reactions occurs shows that the flame structure and propagation velocity are dominated by the decay of $O_3$ into $O_2$ and O and the recombination of O with $O_3$ to form $O_2$. This result was also confirmed in our numerical calculations. It was also found that the small concentrations of O recombined with themselves to form $O_2$ only after the mixture was nearly burned.

Similar results were found by Meintjes[6] who employed 121 grid points and an explicit predictor–corrector method. He also found that the atomic oxygen mass fraction presented a peak equal to $(0.45 \pm 0.011) \times 10^{-3}$ just behind the flame. This peak should be compared with that of Margolis,[4] i.e. with $4.51 \times 10^{-3}$.

Reitz[5] also studied the ozone-decomposition flame by means of an adaptive Saul'yev technique and found good agreement between his results and those of Margolis[4] except for the flame location because of differences in the steady state laminar flame speed. Reitz[5] results also show that the atomic oxygen mass fraction behind the flame front is slightly larger than that of Margolis.[4] Thus Reitz[5] results are in agreement with our findings.

In the steady state, equation (11) has a travelling wave solution whose speed can be calculated by employing the following equation

$$\frac{\partial Y_j}{\partial t^*} + S\frac{\partial Y_j}{\partial \Psi} = 0, \quad j = 1, 2 \tag{38}$$

where $S$ is the steady state laminar flame speed. Substituting the values of $\partial Y_j/\partial t^*$ given by equation (38) into equation (11), and integrating the resulting equation we obtain

$$S[Y_j(t^*, -\infty) - Y_j(t^*, \infty)] = \int_{-\infty}^{\infty} \frac{\omega_i}{\rho} d\Psi, \quad j = 1, 2 \tag{39}$$

where the following boundary conditions have been used at $\Psi = -\infty$ and $\Psi = \infty$

$$\frac{\partial T}{\partial \Psi} = \frac{\partial Y_j}{\partial \Psi} = 0, \quad j = 1, 2 \tag{40}$$

The value of $S$ was calculated from equation (39) according to the numerical schemes described before. This value corresponds to 49·57, 49·51, 48·91, 48·97 and 49·38 cm/s for the fourth-order accurate method of lines, majorant operator-splitting method, first, second, and third time-linearization schemes, respectively. The accuracy of the time-linearization schemes increases when the magnitudes of the spatial and temporal truncation errors decrease. For example, the first and second time-linearization schemes are both second-order accurate in space, and first- and second-order accurate in time. They yield flame speeds of 48·91 and 48·97 cm/s, respectively. These results indicate that the temporal approximation is not as important as the spatial discretization; this is not surprising since a time step equal to 1 $\mu$s was used in the calculations. There is substantial accuracy improvement when fourth-order accurate spatial approximations are employed. This can easily be seen by comparing the flame speed computed with the second time-linearization scheme (48·91 cm/s) with that of the third time-linearization method (49·38 cm/s) and those of the method of lines (49·57 cm/s) and majorant operator-splitting method (49·51 cm/s). These results also indicate that an increase in the temporal resolution improves the value of the computed flame speed. For example, the third time-linearization scheme which is second-order accurate in time

Table I. The efficiency of the numerical methods

| Method | Wave speed (cm/s) | CPU time* |
|---|---|---|
| First time-linearization | 48·91 | 1.00 |
| Second time-linearization | 48·97 | 1·06 |
| Third time-linearization | 49·38 | 3·88 |
| Majorant operator-splitting | 49·51 | 2·15 |
| Method of lines | 49·57 | 4·28 |

* Unity corresponds to 203 minutes of central processing unit time in a DEC-20 computer.

yields a slower flame than the fourth-order accurate method of lines which is fourth-order accurate in time. However, as we mentioned before, the temporal accuracy does not play as an important role as the spatial accuracy since the time step employed in the calculations is small.

The efficiency of the numerical methods employed in this study is shown in Table I which represents the wave speeds and CPU times. The CPU times have been normalized by the CPU time of the first time-linearization algorithm, i.e. equations (27) and (28), and correspond to computations performed with a time step equal to 1 $\mu$s and carried out until a time equal to 2057 $\mu$s. By this time, all the numerical methods have reached a steady-state wave speed. The calculations were performed on a DEC-20 computer.

As shown in Table I, the flame speeds computed with different numerical methods differ by less than 2 per cent from each other. Thus, the CPU times presented in Table I can be interpreted as the computational times required by different numerical methods to obtain the same (within 2 per cent) steady-state wave speed, i.e. the same accuracy. Table I indicates that the first and second time-linearization schemes are more efficient than fourth-order accurate methods. The fourth-order accurate majorant operator-splitting method is also very efficient but not as efficient as the first and second time-linearization schemes. This is because the operator-splitting method solves a sequence of two operators (cf. equations (20) and (21)) the solution of which is more expensive than the solution of only one operator. However, these costs decrease by using larger time steps in the solution of the diffusion operator (equation (21)). The third time-linearization method and the method of lines which are fourth-order accurate in space require more computational time than the other methods to achieve the same accuracy. This is because of the large number of non-linearly coupled ordinary differential equations in the method of lines (equation (19)), and the linearization and discretization of the non-linear source terms in the third time-linearization algorithm (equation (32)). It should be pointed out that in equation (32) the source terms $S$ have to be discretized and then linearized as indicated in equation (28). The linearization was performed analytically but requires a large number of multiplications and divisions at three grid points, i.e. at $i - 1, i$ and $i + 1$. Furthermore, the source terms are highly non-linear functions of the temperature, e.g. equation (17), whose linearization and evaluation at three grid points is much more costly than the evaluation of the source term at only one point as required by the first and second time-linearization algorithms, i.e. equations (27), (28) and (29).

The flame speeds computed in the present study compare favourably with those obtained by Margolis[4] and Reitz.[5] The flame speed calculated by Margolis[4] is 49·7 cm/s and may be more accurate than our computed value since he used 270 breakpoints and sixth-order splines. The fourth-order accurate methods employed in this study yield results in close agreement with those of Margolis,[4] but predict higher flame speeds than that computed by Bledjian[3] who calculated a flame speed of 54 cm/s and found that this value depended on which species was used. This seems to

be due to the fact that he did not obtain a steady-state flame propagation. Bledjian's[3] flame speed is also higher than those computed with the second-order methods presented in this paper.

A flame speed of 48 cm/s ($\pm$ 2 cm/s) was found by Meintjes[6] who employed a second-order accurate explicit predictor–corrector method. He found that his wave speed may be in error by about 2 cm/s because he inverted the transformation given by equations (8) and (9) in order to calculate the flame speed. A similar method was employed by Margolis[4] who studied a burner-stabilized flat flame. Our numerical methods do not require the calculation of the fluid velocity $u$ since the flame speed is calculated in mass co-ordinates through equation (39), which does not involve the fluid velocity.

The flame speed computed by Reitz[5] using an adaptive finite-difference scheme is about 49·8 $\pm$ 0·1 cm/s and is in close agreement with that computed by Margolis[4] and the fourth-order accurate methods employed in the present study. The flame speeds based on the ozone and oxygen mass fractions differ from each other by less than 0·01 cm/s so that we can conclude that our speeds are the steady-state flame speeds.

Although the flame speeds predicted by the time-linearization schemes employed in this study, particularly the fourth-order accurate method, are in very good agreement with those computed by using the method of lines, it cannot be concluded that time-linearization methods are as accurate as other numerical schemes. In the particular case considered here, the linearization of the highly non-linear terms seems to be appropriate due to the small time steps employed in the calculations. However, the accuracy of the time-linearization schemes deteriorates when large time steps are considered; in some cases, the linearization of the reaction terms may not yield a diagonally dominant matrix. This may be a problem for some matrix inversion algorithms. The accuracy of the majorant operator-splitting method is very much dependent on the time step used in the calculations; large times uncouple the reaction and diffusion processes and may yield complete instability.

## CONCLUSIONS

The ozone-decomposition laminar flame has been calculated by means of a fourth-order accurate method of lines, a fourth-order accurate operator-splitting algorithm, and a fourth-order accurate time-linearization scheme. Two second-order accurate time-linearization schemes have also been used to compute the species mass fractions and temperature profiles, and the laminar flame speed. It is shown that second-order schemes predict lower flame speeds than fourth-order accurate methods, and that the temporal approximations do not play as an important role as the spatial approximations in determining the accuracy of flame propagation problems which require small time steps.

The numerical results are in good agreement with those obtained by means of finite-element and adaptive grid finite-difference algorithms when fourth-order accurate schemes are employed. The results obtained with second-order methods are in good agreement with those of second-order accurate explicit predictor–corrector schemes, but are lower than those obtained with a second-order accurate method of lines.

## REFERENCES

1. J. I. Ramos, 'Numerical studies of laminar flame propagation in spherical bombs', *AIAA Journal*, **21**, 415–422 (1983).
2. D. N. Lee and J. I. Ramos, 'Application of the finite element method to one-dimensional flame propagation problems', *AIAA Journal*, **21**, 262–269 (1983).
3. L. Bledjian, 'Computation of time-dependent laminar flame structure', *Combustion and Flame*, **20**, 5–17 (1973).
4. S. B. Margolis, 'Time-dependent solution of a premixed laminar flame', *Journal of Computational Physics*, **27**, 410–427 (1978).

5. R. D. Reitz, 'The application of an explicit numerical method to a reaction–diffusion system in combustion', The Courant Institute of Mathematical Sciences, New York University, New York, 1979.

6. K. Meintjes, 'Predictor–corrector methods for time dependent compressible flows', *Ph.D. Thesis*, Princeton University, Princeton, New Jersey, (1979).

7. F. Cramarossa and G. Dixon-Lewis, 'Ozone decomposition in relation to the problem of the existence of steady-state flames', *Combustion and Flame*, **16**, 243–251 (1971).

8. J. Warnatz, 'Calculation of the structure of laminar flat flames I: flame velocity of freely propagating ozone decomposition flames', *Ber. Bunsenges Phys. Chem.*, **82**, 193–200 (1978).

9. J. M. Heimerl and T. P. Coffee, 'The detailed modeling of premixed, laminar steady-state flames I: ozone', *Combustion and Flame*, **39**, 301–315 (1980).

10. B. K. Madsen and R. F. Sincovec, 'PDECOL: general collocation software for partial differential equations', Lawrence Livermore Laboratory, Livermore, California, *Preprint UCRL-78263 (Rev. 1)*, (1977).

11. T. P. Coffee and J. M. Heimerl, 'Sensitivity analysis for premixed, laminar, steady state flames', *Combustion and Flame*, **50**, 323–340 (1983).

12. T. P. Coffee and J. M. Heimerl, 'Transport algorithms for premixed, laminar steady-state flames', *Combustion and Flame*, **43**, 273–289 (1981).

13. G. Tsatsaronis, Prediction of propagating laminar flames in methane, oxygen, nitrogen mixtures', *Combustion and Flame*, **33**, 217–239 (1978).

14. L. D. Smoot, W. C. Hecker and G. A. Williams, 'Prediction of propagating methane–air flames', *Combustion and Flame*, **26**, 323–342 (1976).

15. J. Warnatz, 'Concentration––, pressure––, and temperature-dependence of the flame velocity in hydrogen–oxygen–nitrogen mixtures', *Combustion Science and Technology*, **26**, 203–213 (1981).

16. J. Warnatz, 'The structure of laminar alkane––, alkene––, and acetylene–flames', *Eighteenth Symposium (International) on Combustion*, The Combustion Institute, Pittsburgh, Pennsylvania, 1981, pp. 369–384.

17. J. Warnatz, 'Flame velocity and structure of laminar hydrocarbon–air flames', in *Combustion in Reactive Systems*, J. R. Bowen, N. Manson, A. K. Oppenhein and R. I. Soloukhin (eds.), *Progress in Aeronautics and Astronautics*, **76**, American Institute of Aeronautics and Astronautics, New York, 1981, pp. 501–521.

18. J. Warnatz, H. Bockhorn, A. Moser and H. W. Wenz, 'Experimental investigations and computational simulation of acetylene–oxygen flames from near stoichiometric to sooting conditions', *Nineteenth Symposium (International) on Combustion*, The Combustion Institute, Pittsburgh, Pennsylvania, 1982, pp. 197–209.

19. J. A. Miller, R. E. Mitchel, M. D. Smooke and R. J. Kee, 'Towards a comprehensive chemical kinetic mechanism for the oxidation of acetylene: comparison of model predictions with results from flame and shock tube experiments', *Nineteenth Symposium (International) on Combustion*, The Combustion Institute, Pittsburgh, Pennsylvania, 1982, pp. 181–196.

20. D. B. Spalding, R. L. Stephenson and R. G. Taylor, 'A calculation procedure for the prediction of laminar flame speeds', *Combustion and Flames*, **17**, 55–64 (1971).

21. R. L. Stephenson and R. G. Taylor, 'Laminar flame propagation in hydrogen, oxygen, nitrogen mixtures', *Combustion and Flame*, **20**, 231–244 (1973).

22. F. A. Williams, *Combustion Theory*, Addison–Wesley Publishing Company, Reading, Massachusetts, 1965.

23. N. N. Yannenko, *The Method of Fractional Steps*, Springer-Verlag, New York, 1971.

24. Z. Kopal, *Numerical Analysis*, Wiley, New York, 1961.

25. R. E. Bellman and R. Kalaba, *Quasilinearization and Nonlinear Boundary Value Problems*, American Elsevier, New York, 1965.

26. W. R. Briley and H. McDonald, 'Solution of the multidimensional compressible Navier–Stokes equations by a generalized implicit method', *Journal of Computational Physics*, **24**, 372–392 (1977).

27. R. M. Beam and R. F. Warming, 'An implicit factored scheme for the compressible Navier–Stokes equations', *AIAA Journal*, **16**, 393–402 (1978).